Inorganic Chemistry

Article

pubs.acs.org/IC

Gallium Arsenate Dihydrate under Pressure: Elastic Properties, Compression Mechanism, and Hydrogen Bonding

Elinor C. Spencer,[†] Victoria Soghomonian,[‡] and Nancy L. Ross*,[†]

[†]Department of Geosciences and [‡]Department of Physics, Virginia Tech, Blacksburg, Virginia 24061, United States

Supporting Information

ABSTRACT: Gallium arsenate dihydrate is a member of a class of isostructural compounds, with the general formula $M^{3+}AsO_4{\cdot}2H_2O$ (M^{3+} = Fe, Al, In, or Ga), which are being considered as potential solid-state storage media for the sequestration of toxic arsenic cations. We report the first high-pressure structural analysis of a metal arsenate dihydrate, namely, $GaAsO_4{\cdot}2H_2O$. This compound crystallizes in the orthorhombic space group *Pbca* with $Z = 8$. Accurate unit cell parameters as a function of pressure were obtained by high-pressure single-crystal X-ray diffraction, and a bulk modulus of 51.1(3) GPa for $GaAsO_4{\cdot}2H_2O$ was determined from a third-order Birch−Murnaghan equation of state fit to the *P*−*V* data. Assessment of the pressure dependencies of the unit cell lengths showed that the compressibility of the structure along the axial directions increases in the order of [010] < [100] < [001]. This order was found to correlate well with the proposed compression mechanism for $GaAsO_4{\cdot}2H_2O$, which involves deformation of the internal channel void spaces of the polyhedral helices that lie parallel to the [010] direction, and increased distortion of the GaO_6 octahedra. The findings of the high-pressure diffraction experiment were further supported by the results from variable-pressure Raman analysis of $GaAsO_4{\cdot}2H_2O$. Moreover, we propose a revised and more complex model for the hydrogen-bonding scheme in $GaAsO_4{\cdot}2H_2O$, and on the basis of this revision, we reassigned the peaks in the OH stretching regions of previously published Raman spectra of this compound.

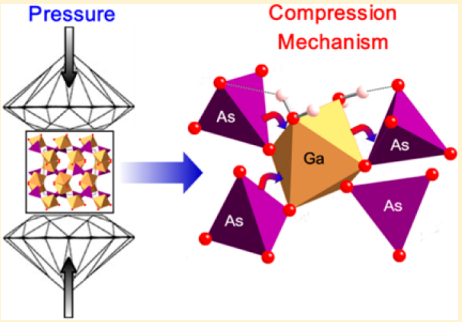

INTRODUCTION

The generation of metal arsenate waste from the processing and mining of arseniferous and precious metal ores and the industrial preparation of semiconductors and other metallurgical products pose a significant risk to the environment and public health.[1−3] Of particular concern is the potential leaching of highly toxic and soluble cationic arsenic from these polluted waste materials and its subsequent entrance into the watercourse.[4] Consequently, there is significant current interest in the preparation of highly stable arsenic containing compounds that effectively immobilize the arsenic, thus enabling the controlled management of this problematic contaminant.

Some of the most promising candidates for this application are metal arsenate dihydrates with the general formula of $M^{3+}AsO_4{\cdot}2H_2O$ (where M^{3+} = Fe, Al, In, or Ga). These compounds are isostructural, and several of them are found as the naturally occurring minerals scorodite ($FeAsO_4{\cdot}2H_2O$), mansfieldite ($AlAsO_4{\cdot}2H_2O$), and yanomamite ($InAsO_4{\cdot}2H_2O$). Gomez et al. have postulated that there is a correlation between the electronegativity of the M^{3+} cation and the overall stability of the $M^{3+}AsO_4{\cdot}2H_2O$ compounds in water.[5,6] These authors proffered this hypothesis based on their results from extensive Raman measurements of a range of $M^{3+}AsO_4{\cdot}2H_2O$ materials that demonstrated a trend in the stretching frequency, and thus strength, of the As−O bonds and the aqueous solubility of these compounds. Indeed, the stability of these compounds was shown to be in the order of $FeAsO_4{\cdot}2H_2O$ < $InAsO_4{\cdot}2H_2O$ < $GaAsO_4{\cdot}2H_2O$ < $AlAsO_4{\cdot}2H_2O$. However, if metal arsenate dihydrates are to be considered for the safe storage of arsenic, then they must demonstrate structural stability under geological conditions. In particular, it is essential that their structural response and resistance to pressure be evaluated fully.

In this contribution, we report a combined high-pressure diffraction and spectroscopic study of gallium arsenate dihydrate. $GaAsO_4{\cdot}2H_2O$ and its isostructural $M^{3+}AsO_4{\cdot}2H_2O$ analogues crystallize in the orthorhombic space group *Pbca* ($Z = 8$). Each AsO_4 tetrahedron shares its vertices with four neighboring GaO_6 octahedra, and the coordination sphere of the Ga^{3+} ions comprises four vertex sharing AsO_4 and two cis-coordinated water molecules. The three-dimensional $GaAsO_4{\cdot}2H_2O$ framework (Figure 1) comprises cross-linked helices of alternating tetrahedra/octahedra, which are generated by the 2_1 screw axes that lie parallel to the crystallographic *b*-axis (Figure 1b). A combination of strong and weak hydrogen bonds confers additional stability to the $GaAsO_4{\cdot}2H_2O$ structure (Figure 2).

EXPERIMENTAL METHODS

Synthesis. The single crystals of $GaAsO_4{\cdot}2H_2O$ employed in this study were a minor product from the hydrothermal preparation of

Received: May 20, 2015
Published: July 20, 2015

DOI: 10.1021/acs.inorgchem.5b01144
Inorg. Chem. 2015, 54, 7548−7554

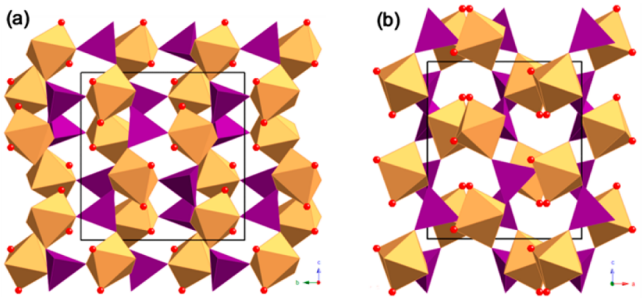

Figure 1. Crystal structure of $GaAsO_4{\cdot}2H_2O$ viewed along the (a) [100] and (b) [010] directions. Light brown octahedra and purple tetrahedra represent GaO_6 and AsO_4 units, respectively. Red spheres depict coordinated water molecules; all other oxygen atoms and hydrogen atoms are omitted for clarity.

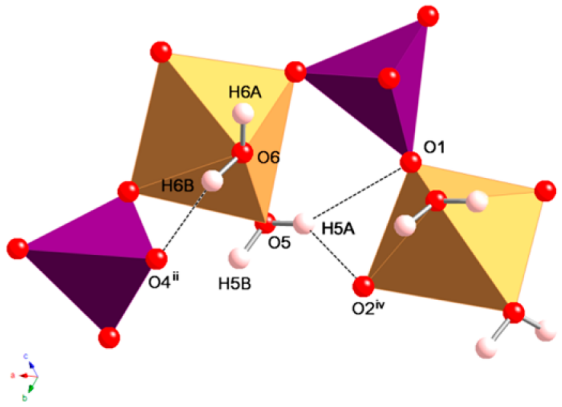

Figure 2. Figure showing the hydrogen bonds (dashed lines) in the crystal structure of $GaAsO_4{\cdot}2H_2O$. Symmetry codes: (ii) $0.5 - x, 0.5 + y, z$; (iv) $-x, 0.5 + y, 1.5 - z$. Light brown octahedra and purple tetrahedra represent GaO_6 and AsO_4 units, respectively. Red and white spheres depict oxygen and hydrogen atoms, respectively. Under ambient conditions, in air: O6···$O4^{ii}$ length = 2.612(3) Å; O6−H6B···$O4^{ii}$ angle = 152.4(2)°; O5···$O2^{iv}$ length = 2.690(3) Å; O5−H5A···$O2^{iv}$ angle = 142.9(2)°; O5···O1 length = 3.004(3) Å; O5−H5A···O1 angle = 133.5(2)°.

vanadium oxide nanostructures.[7] In summary, an aqueous solution of hydrolyzed VCl_4, $Na_2HAsO_4{\cdot}7H_2O$, $GaCl_3$, and guanidinium hydrochloride, in a mole ratio of 252:1:3.75:5.78, was placed in a Parr bomb and heated at 456 K for 90 h before being cooled to room temperature. Perfect colorless octahedral crystals of $GaAsO_4{\cdot}2H_2O$ were hand-separated from the vanadium oxide nanosheets that are the major product of this reaction. ***Caution!*** *The reactants should be weighed and manipulated in a fume hood to minimize expose to arsenic containing compounds. Hydrolysed VCl_4 solution should be prepared in an ice bath placed in a fume hood to mitigate the violent exothermic reaction that generates HCl; the resultant product is a stable blue solution, which contains the VO^{+2} species.*

High-Pressure Diffraction. A single crystal of $GaAsO_4{\cdot}2H_2O$ ($100 \times 89 \times 73$ μm^3) was loaded in a standard ETH diamond anvil cell (DAC) with an opening angle of 40° and fitted with a steel gasket.[8] A chamber (400×130 μm^2) had been drilled in the gasket to hold both the sample crystal and a quartz crystal. The quartz crystal was included in the cell to act as a pressure calibrant.[9] After diffraction data were collected under ambient conditions, a 4:1 methanol/ethanol mixture was added to the DAC to act as the pressure-transmitting medium. This alcohol mixture is known to remain hydrostatic up to 9.8 GPa.[10]

Precise unit cell parameters for both the $GaAsO_4{\cdot}2H_2O$ and quartz crystals were determined with a Huber diffractometer equipped with an Eulerian cradle and point detector. The method employed for the determination of the unit cell parameters was based on the eight-position centring of 12−25 intense diffraction maxima within the $9° < 2\theta < 33°$ range.[11]

Diffraction data for structure analysis were recorded at selected pressure points on an XCalibur-1 diffractometer equipped with a CCD detector and operating with monochromated Mo Kα radiation (λ = 0.710 73 Å). The data were processed with standard instrument software. Absorption by the sample and DAC components were corrected for with ABSORB-7,[12] and the data were corrected for DAC dips and other anomalies with AVERAGE (R. J. Angel, 2003−2011). Structural solution was performed with data collected under ambient conditions and by direct methods. High-pressure structures were determined from refinement of this initial starting structure; this was possible because no phase transitions occurred over the pressure range investigated. Refinement was against F^2 by full-matrix least-squares refinement techniques. Because of the restricted access to reciprocal space, only ~60% of the unique data for $GaAsO_4{\cdot}2H_2O$ were collected. Therefore, the refinements of all the high-pressure structures were, by necessity, isotropic. However, the only constraints/restraints applied to the models were bond length and angle restraints involving

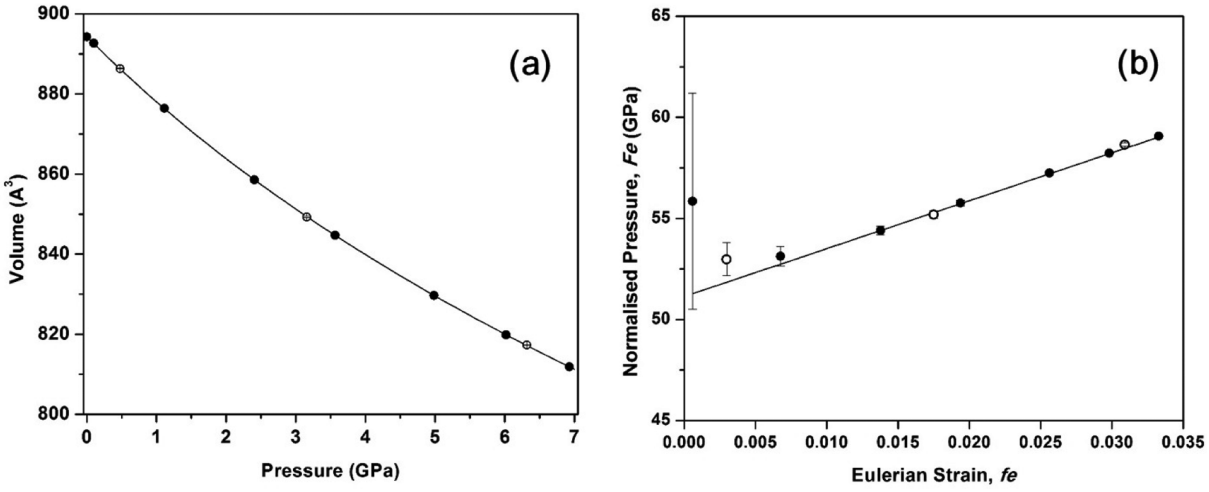

Figure 3. (a) Unit cell volume vs pressure data for $GaAsO_4{\cdot}2H_2O$. Error bars are included in this plot, but are smaller than the symbols. (b) F_e vs f_e plot for $GaAsO_4{\cdot}2H_2O$. In both (a) and (b) the solid curves are the calculated third-order Birch−Murnaghan equation of state fits to the data. Filled and open circles represent data collected during pressure increase and decrease, respectively.

DOI: 10.1021/acs.inorgchem.5b01144
Inorg. Chem. 2015, 54, 7548−7554

the hydrogen atoms of the coordinated water molecules. Additional crystallographic information is available in the Supporting Information.

High-Pressure Raman Spectroscopy. A $GaAsO_4{\cdot}2H_2O$ crystal was loaded into a Brillouin-Raman (BR-series) DAC (High-Pressure Diamond Optics, Inc.). This DAC was fitted with two type-IIa diamonds, both 600 μm in diameter. Diamonds of this class contain low levels of impurities and therefore display negligible photoluminescence. The DAC was fitted with a stainless-steel gasket in which a sample chamber with dimensions of 250 × 100 μm^2 was drilled. Upon closure of the DAC, the $GaAsO_4{\cdot}2H_2O$ crystal was crushed to give a microcrystalline material. A 4:1 methanol/ethanol mixture was employed as the pressure-transmitting medium. A ruby ball was placed in the DAC sample chamber for pressure calibration measurements.[13]

High-pressure Raman spectra for $GaAsO_4{\cdot}2H_2O$ were recorded at room temperature on a JY Horiba LabRam HR spectrometer operating with a 40× objective and equipped with a red laser (λ = 632.817 nm). The spectral slits were 150 μm in size, and the confocal hole was set to 400 μm. The spectrograph grating had 1200 grooves/mm. Each data acquisition comprised two scans each of which was 60 s in duration. The photoluminescence signals (at ca. 694 nm) of the ruby were measured under the same experimental conditions as those used for the $GaAsO_4{\cdot}2H_2O$ measurements except that the scans lengths were varied to reduce/increase the signal strength when required.

RESULTS AND DISCUSSION

Elastic Properties. Figure 3 shows the pressure dependency of the unit cell volume of $GaAsO_4{\cdot}2H_2O$ and the associated normalized pressure versus Eulerian strain data (F_e vs f_e plot). These data unequivocally show that $GaAsO_4{\cdot}2H_2O$ undergoes no phase transitions within the 0−7 GPa pressure range; moreover, this arsenate demonstrates fully reversible and continuous compression up to 7 GPa.

The unit cell volume versus pressure (V−P) data and the unit cell lengths versus pressure data (Figure 4) have been fitted with third-order Birch−Murnaghan equations of state,[14] and from these calculations the elastic constants for $GaAsO_4{\cdot}2H_2O$ have been evaluated (Table 1). To the best of our knowledge, the only other $M^{3+}AsO_4{\cdot}2H_2O$ compound for which elastic constants have been published is the iron analogue scorodite ($FeAsO_4{\cdot}2H_2O$) for which V_0 = 934.2(3) Å^3; K_0 = 62(3) GPa; K' = 6.6(9).[15] Unfortunately, because of the large error on the reported bulk modulus of $FeAsO_4{\cdot}2H_2O$, we cannot say with any statistical certainty that bulk modulus for $GaAsO_4{\cdot}2H_2O$ (51.1(3) GPa) is any different from that of scorodite. Nonetheless, the values are suggestive and imply that $FeAsO_4{\cdot}2H_2O$ exhibits a greater resistance to pressure than $GaAsO_4{\cdot}2H_2O$, which concurs with the $M^{3+}AsO_4{\cdot}2H_2O$ stability trend predicted by Gomez et al.[5] For further comparison, the low-pressure form of anhydrous gallium arsenate, $GaAsO_4$ (α-quartz type), has a K_0 value of 32.0 GPa.[16] Unfortunately, no elastic data for the closely related gallium phosphate dihydrate, $GaPO_4{\cdot}2H_2O$, are available for comparison with our results.

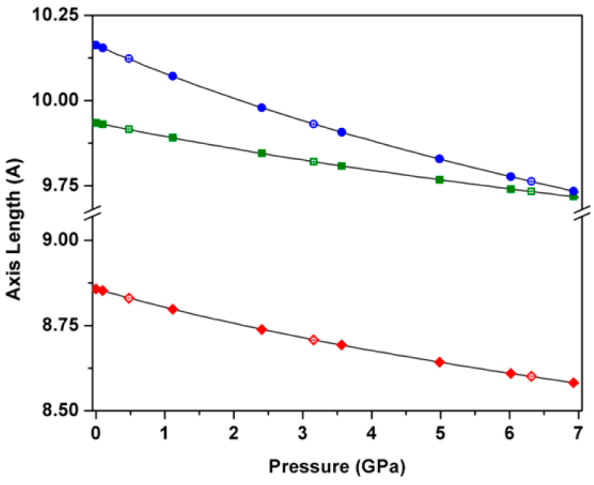

Figure 4. Unit cell axes lengths vs pressure data for $GaAsO_4{\cdot}2H_2O$ (red diamonds: *a*-axis; green squares: *b*-axis; blue circles: *c*-axis). Filled and open symbols represent data collected during pressure increase and decrease, respectively. Error bars are included in this plot but are smaller than the symbols. The solid curves are the calculated third-order Birch−Murnaghan equation of state fits to the data.

The axial bulk moduli are also reported in Table 1. These values indicate that, when subjected to hydrostatic pressure, the contraction of the $GaAsO_4{\cdot}2H_2O$ unit cell is anisotropic. Furthermore, compressibility ($\beta_i = M_i^{-1}$) along the axial directions increases in the order of [010] < [100] < [001]. This implies that compression along the axes of the polyhedral helices that lie parallel to [010] is unfavorable with respect to compression in directions perpendicular to these helices.

Compression Mechanism. The crystal structure of $GaAsO_4{\cdot}2H_2O$ was determined at selected pressures (Table 2), and Table 3 shows the evolution of key bond lengths and angles for this compound with pressure. No statistically significant change is seen in the internal bond parameters of the AsO_4 tetrahedra over the pressure range investigated; therefore, these polyhedra can be considered to behave as rigid units in response to pressure, at least up to 7 GPa. The same assumption cannot be applied to the GaO_6 octahedra. All the significant changes in bond parameters that occur in response to pressure are associated with either the interpolyhedral angles (As−O−Ga) or adjustments to the geometry of the distorted GaO_6 octahedra (Table 3).

The deviation of the GaO_6 octahedra from ideal O_h geometry can be quantified by the variation in the octahedral angles ($\sigma_{\theta(oct)}{}^2$) and the mean octahedral quadratic elongation parameter ($\langle\lambda_{oct}\rangle$).[17] The latter distortion parameter is a measure of the deviation of the experimentally determined bond lengths from the center-to-vertex distance (l_0) for an octahedron of equivalent volume and O_h symmetry; for an idea octahedron $\sigma_{\theta(oct)}{}^2 = 0$ and $\langle\lambda_{oct}\rangle = 1$. These distortion parameters for the GaO_6 octahedra have been quantified, and are reported in Table 4. The $\langle\lambda_{oct}\rangle$ parameter remains approximately equal to unity over the 0−7 GPa pressure range, which indicates that the observed reduction in octahedral volume (V_{oct}) that accompanies this pressure change is not a consequence of changes in the Ga−O bond lengths. Indeed, the data in Table 3 show that only one Ga−O bond contracts with pressure, while the other Ga−O distances remain constant. However, the angular variance indicates that even at room pressure the GaO_6 octahedra are severely distorted, and the accumulative degree of angular distortion that occurs with increasing pressure drives the reduction in V_{oct}.

Given that four of the oxygen atoms of the GaO_6 octahedra are the vertices of neighboring AsO_4 tetrahedra, it is not surprising that the pressure-induced distortions to the GaO_6 octahedra occur concomitantly with changes in the As−O−Ga interpolyhedral angles (Figure 5). Reduction of the As1^{i}−O1^{i}−Ga1, As1^{ii}−O2^{ii}−Ga1, and As1−O4−Ga1 (see Table 3 for symmetry codes) angles will result in a small distortion of the shape of the helices (Figure 1b) that is manifest as

DOI: 10.1021/acs.inorgchem.5b01144
Inorg. Chem. 2015, 54, 7548−7554

Table 1. Elastic Constants for $GaAsO_4{\cdot}2H_2O$ Derived from the Third-Order Birch−Murnaghan Equation of State Fits to the Variable-Pressure Unit Cell Parameters

			a-axis	*b*-axis	*c*-axis
V_0 (Å^3)	894.29(7)	X_0 (Å)	8.8577(3)	9.9349(3)	10.1625(4)
K_0 (GPa)	51.1(3)	M_0 (GPa)	152(1)	233(2)	115(1)
K'	7.1(2)	M'	23.5(5)	28(1)	15.7(5)
K'' (GPa^{-1})	−0.32316	M'' (GPa^{-1})	−1.37261	−1.41174	−0.52534

Table 2. Refinement and Data Details for Variable Pressure (GPa) $GaAsO_4{\cdot}2H_2O$ Diffraction Data

	ambient	2.405(6)	4.985(7)	6.927(8)
crystal system	orthorhombic	orthorhombic	orthorhombic	orthorhombic
space group	*Pbca*	*Pbca*	*Pbca*	*Pbca*
a (Å)	8.8574(4)	8.7386(4)	8.6425(3)	8.5822(3)
b (Å)	9.9347(4)	9.8454(4)	9.7675(3)	9.7183(3)
c (Å)	10.1625(2)	9.979(1)	9.8284(9)	9.7342(9)
V (Å^3)	894.25(5)	858.5(1)	829.68(9)	811.87(8)
ρ (g/cm^3)	3.635	3.786	3.918	4.003
independent reflns	1273	832	786	772
R_{int}	0.240	0.314	0.357	0.318
data/parameters[a]	827/34	453/42	428/42	421/41
S	0.887	0.891	0.942	0.889
*R*1 ($I > 2\sigma I$)	0.0814	0.0863	0.1058	0.0806
*wR*2 ($I > 2\sigma I$)	0.1750	0.1712	0.2413	0.1802

[a]Differences in the number of refined parameters are due to type of hydrogen atom restraints/constraints applied in the models. Variation was necessary to ensure convergence of the refinements.

compression, principally in the [001] direction, of the internal channel space. If this mechanism were operating alone, then one can envisage that compression of the void channel along [001] would necessitate expansion in the perpendicular [100] and [010] directions. However, the concurrent decrease in the volume of the GaO_6 octahedra (V_{oct}) ensures that this distortion is compensated for and allows for contraction rather than expansion along the [100] and [010] directions. This proposed compression mechanism for $GaAsO_4{\cdot}2H_2O$ is consistent with the measured elastic constants (Table 1) for this compound, which indicate that compressibility along the crystallographic axes increases in the order of [010] < [100] < [001] (vide supra).

The subtlety of the changes in the structure with pressure is evident in the high-pressure Raman spectra of $GaAsO_4{\cdot}2H_2O$, Figure 6a. Below 300 cm^{-1} the spectra are dominated by signals arising from the lattice modes. Peaks in the 300−500 cm^{-1} regions correspond to the internal deformation/bending modes of the AsO_4 and GaO_6 polyhedra, and the broad strong features in the 800−1000 cm^{-1} sections of the spectra relate to the stretching vibrations of the AsO_4 tetrahedra and the deformation modes of the Ga−(OH_2) moieties. The Ga−O stretching modes occupy the 600−800 cm^{-1} regions of the spectra.[5,6,18,19] There are no significant differences in the variable pressure spectra below 500 cm^{-1}, indicating that the Raman measurements are insensitive to the pressure-induced internal distortions of the GaO_6 octahedra that were clearly evident in the high-pressure diffraction measurements. However, there is a clear redistribution of intensity of the broad combination band at ca. 930 cm^{-1} as the pressure is increased. This is a consequence of the pressure-induced changes in the environment of the AsO_4 tetrahedra that are caused by alterations in the As−O−Ga interpolyhedral angles, and the distortions of the GaO_6 octahedra that influence the deformation modes of the Ga−(OH_2) units. Although there are multiple peaks in the Ga−O stretching regions of the spectra, they are poorly resolved, and the intensity is low; consequently, the pressure-induced changes to the GaO_6 octahedra that were observed in the diffraction data cannot be resolved in the Raman spectra. Above ca. 5.1 GPa the quality of the Raman spectra deteriorates such that they no longer provide useful structural information.

Regrettably, hitherto no high-pressure structural data for any of the isostructural $M^{3+}AsO_4{\cdot}2H_2O$ analogous of $GaAsO_4{\cdot}2H_2O$ have been published, and therefore we are unable to compare this mechanism with others that may operate within this class of compound or determine if the physical properties of the M^{3+} cation influences the resistance of hydrated metal arsenates to pressure.

Hydrogen Bonding. Raman measurements by Gomez et al.[5] displayed one sharp and one broad peak in the 3000−3575 cm^{-1} regions of the Raman spectra of $GaAsO_4{\cdot}2H_2O$. These stretching peaks were assigned to water O−H bonds participating in two hydrogen-bonding environments in the $GaAsO_4{\cdot}2H_2O$ structure: strong (broad, 3002 cm^{-1}) and weak (sharp, 3482 cm^{-1}). However, these authors incorrectly defined the hydrogen-bond network in the $M^{3+}AsO_4{\cdot}2H_2O$ family of compounds. There are in fact three distinct OH environments in the $GaAsO_4{\cdot}2H_2O$ structure (Figure 2): (i) OH groups not participating in hydrogen bonding, i.e., donor···acceptor (D···A) distances greater than 3.1 Å (O6−H6A and O5−H6B); (ii) OH groups involved in bifurcated hydrogen bonding comprising both strong and weak interactions (O5−H6A); and (iii) OH groups participating in strong hydrogen bonding (O6−H6B). We therefore tentatively reassign the sharp peak at 3482 cm^{-1} observed in the spectra reported by Gomez et al. as originating from the stretching vibrations of the non-hydrogen-bonded OH bonds of the coordinated molecules and the broad band at 3002 cm^{-1} as a combination band associated with the stretching vibrations of OH groups in *both* hydrogen-bonded

DOI: 10.1021/acs.inorgchem.5b01144
Inorg. Chem. 2015, 54, 7548−7554

Table 3. Selected Bond Lengths (Å) and Angles (deg) for $GaAsO_4{\cdot}2H_2O$ as a Function of Pressure (GPa)[a]

	ambient	2.405(6)	4.985(7)	6.927(8)
As1−O1	1.68(2)	1.72(3)	1.71(5)	1.72(3)
As1−O2	1.68(2)	1.66(2)	1.65(3)	1.69(2)
As1−O3	1.68(2)	1.73(2)	1.68(4)	1.69(2)
As1−O4	1.72(2)	1.67(2)	1.67(3)	1.69(2)
Ga1−O1^{i}	1.96(2)	1.93(2)	1.96(3)	1.92(2)
Ga1−O2^{ii}	1.97(2)	1.99(2)	1.98(3)	1.93(2)
Ga1−O3^{iii}	1.93(2)	1.87(3)	1.85(5)	1.86(3)
Ga1−O4	1.90(2)	1.95(2)	1.91(3)	1.91(2)
Ga1−O5	**2.01(1)**	**1.94(3)**	**1.93(3)**	**1.86(2)**
Ga1−O6	2.09(2)	2.06(2)	2.05(3)	2.06(2)
O1−As1−O2	113.8(8)	114(1)	115(2)	115(1)
O1−As1−O4	107.2(9)	110(1)	109(2)	111(1)
O2−As1−O4	108.0(9)	106.8(9)	107(2)	106(1)
O3−As1−O1	106.3(9)	107(1)	108(2)	106(1)
O3−As1−O2	108.4(9)	108(1)	106(2)	106(1)
O3−As1−O4	113.3(9	111(1)	112(2)	113(1)
As1^{i}−O1^{i}−Ga1	**132(1)**	**128(1)**	**125(2)**	**126(2)**
As1^{ii}−O2^{ii}−Ga1	**131(1)**	**128(1)**	**127(1)**	**126(1)**
As1^{iii}−O3^{iii}−Ga1	133(1)	131(1)	133(2)	132(1)
As1−O4−Ga1	**134(1)**	**131(1)**	**131(2)**	**128(1)**
O1^{i}−Ga1−O2^{ii}	87.9(8)	89.0(8)	87(1)	86.2(9)
O1^{i}−Ga1−O5	**97.4(6)**	**102(1)**	**102(2)**	**103(1)**
O1^{i}−Ga1−O6	**176.5(7)**	**172.2(9)**	**170(1)**	**170(1)**
O2^{ii}−Ga1−O5	84.7(6)	85.3(9)	83(2)	83(1)
O2^{ii}−Ga1−O6	**95.6(8)**	**98.2(8)**	**101(1)**	**101.4(8)**
O3^{iii}−Ga1−O1^{i}	**93.3(7)**	**88(1)**	**88(2)**	**87(1)**
O3^{iii}−Ga1−O2^{ii}	91.1(7)	90.6(9)	89(2)	89(1)
O3^{iii}−Ga1−O5	168.4(7)	169.2(9)	167(1)	167(1)
O3^{iii}−Ga1−O6	86.8(7)	88.5(9)	86(2)	86.3(9)
O4−Ga1−O1^{i}	**89.7(8)**	**86.1(8)**	**86(1)**	**83.6(9)**
O4−Ga1−O2^{ii}	**177.5(8)**	**174.5(8)**	**173(1)**	**169.5(8)**
O4−Ga1−O3^{iii}	88.0(8)	87(1)	89(2)	88(1)
O4−Ga1−O5	**96.6(7)**	**98.0(9)**	**100(2)**	**102(1)**
O4−Ga1−O6	86.7(7)	86.7(8)	85(1)	88.4(8)
O5−Ga1−O6	82.8(6)	82.2(9)	86(1)	85.3(9)

[a]Symmetry codes: (i) $x + 0.5, y, 1.5 - z$; (ii) $0.5 - x, y + 0.5, z$; (iii) $x + 0.5, 1.5 - y, 1 - z$. Parameters that display a statistically significant change over the 0−7 GPa pressure range are in bold type. Atom labelling scheme is shown in Figure 5.

Table 4. Measured Volume and Distortion Parameters for the GaO_6 Octahedra as a Function of Pressure

pressure (GPa)	GaO_6 V_{oct} (Å^3)	$V_{oct}/(V_{oct})_0$	l_0 (Å^3)	$\langle\lambda_{oct}\rangle$	$\sigma_{\theta(oct)}{}^2$
ambient	10.189	1	1.97	1.008	22.849
2.405(6)	9.820	0.96	1.95	1.008	36.444
4.985(7)	9.635	0.94	1.93	1.018	46.455
6.927(8)	9.272	0.91	1.91	1.015	54.518

environments (denoted as (ii) and (iii) above). These revised assignments are consistent with the expected peak positions for the stretching vibrations of strongly hydrogen-bonded OH groups, as detailed by Libowitsky and others.[20,21]

Unfortunately, because of interference from the diamonds of the DAC and the methanol/ethanol pressure medium, data in the 1100−3100 cm^{-1} range are inaccessible in our high-pressure measurements; consequently, we can only assess the pressure-induced behavior of the peaks relating to the non-hydrogen-bonded OH groups of the coordinated molecules. These peaks (Figure 6b) are of low intensity, and these regions

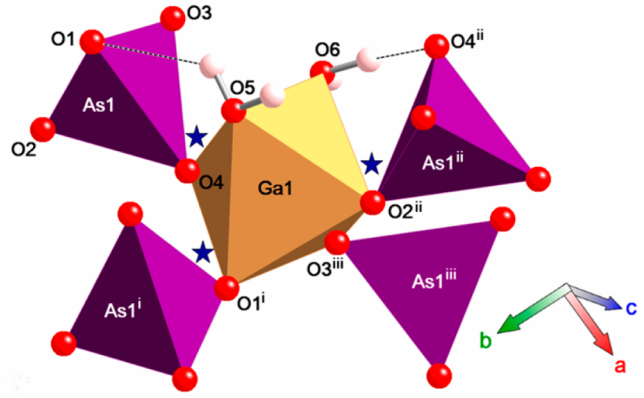

Figure 5. Figure showing the atom labeling scheme. As−O−Ga bridges that flex in response to pressure resulting in reduction in the As−O−Ga angles are indicated by stars. See Table 3 for symmetry codes. The unit cell basis is also shown. Hydrogen bonds are shown as dashed lines.

of the spectra are also subject to high levels of noise. Nonetheless, the bands were fitted with Gaussian functions, the details of which are reported in Table 5. The appropriateness of this fitting procedure is highlighted by the excellent agreement of the central position determined for the peak recorded under ambient conditions, 3484.45(1) cm^{-1}, with the value reported by Gomez et al., 3482 cm^{-1}. This peak undergoes an impressive 201 cm^{-1} blueshift as the pressure is increased to 5.106 GPa. This is indicative of the coordinated water molecules experiencing pressure-induced alterations in their chemical environments. This conclusion is supported by the high-pressure diffraction results, which show increased distortion of the GaO_6 octahedra, including a significant reduction in the Ga−O(5)H_2 bond length (Table 3) with increasing pressure.

Table 6 provides details of the D···A distances, determined from the high-pressure diffraction data, associated with the hydrogen-bonded OH groups in the solid-state structure of $GaAsO_4{\cdot}2H_2O$. It can be envisaged that the reduction in the Ga1−O4−As1 and As1^{ii}−O2^{ii}−Ga1 angles (Figure 5, Table 3) with increasing pressure would strengthen the hydrogen bonds by decreasing the D···A distances. However, no statistically significant changes in the D···A distances are observable. This may be a consequence of the large estimated standard deviation values on the refined D···A distances prohibiting detection of the expected changes to the hydrogen-bond network.

CONCLUSION

In this contribution we have reported the first high-pressure structural analysis of an $M^{3+}AsO_4{\cdot}2H_2O$ compound. By fitting the measured $P-V$ data with a third-order Birch−Murnaghan equation of state the bulk modulus for $GaAsO_4{\cdot}2H_2O$ was calculated to be 51.1(3) GPa. To place this value in context, ca. 60% of the Earth's crust is comprised of feldspar minerals that typically exhibit bulk moduli within the 50−80 GPa range.[22−24] This suggests that $GaAsO_4{\cdot}2H_2O$, and possibly other analogous $M^{3+}AsO_4{\cdot}2H_2O$ compounds, can demonstrate sufficient resistance to geological pressures to warrant their continued consideration as potential materials for arsenic sequestration.

In addition to deriving accurate elastic constants for $GaAsO_4{\cdot}2H_2O$, we have ascertained that compression of this compound is facilitated by adjustments in the As−O−Ga interpolyhedral linkages and significant deformation of the GaO_6 octahedra,

DOI: 10.1021/acs.inorgchem.5b01144
Inorg. Chem. 2015, 54, 7548−7554

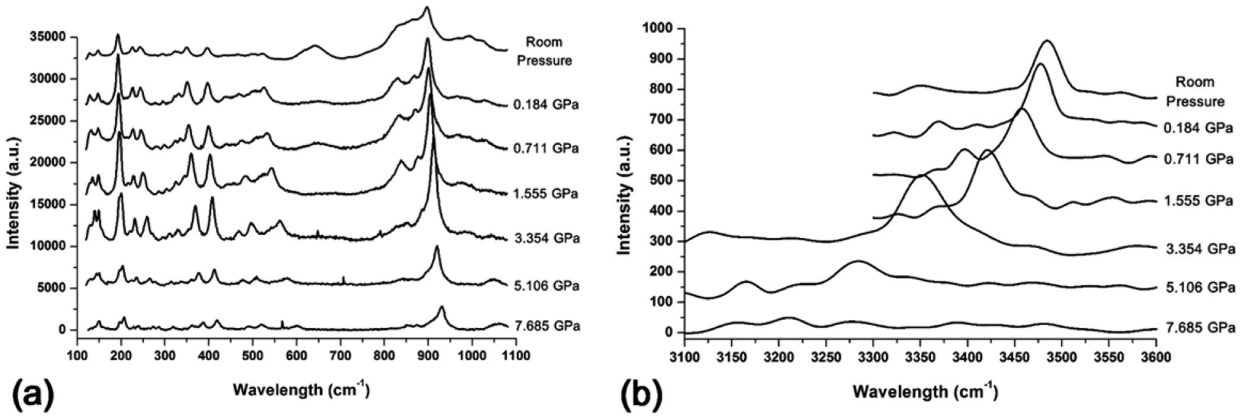

Figure 6. High-pressure Raman spectra for $GaAsO_4{\cdot}2H_2O$: (a) 100−1100 cm^{-1} range; (b) 3100−3600 cm^{-1} range. Because of high levels of background noise and the low intensities of the peaks in the 3100−3600 cm^{-1} regions, these spectra were smoothed with a Savitzky−Golay function to enable observation of the spectral features. Data in the 1100−3100 cm^{-1} range were not measured due to interference from signals from the DAC diamonds and alcohol pressure medium.

Table 5. Position and Frequency Half-Width Maximum (FHWM) Values of the Stretching Band for Non-Hydrogen-Bonded OH Groups as a Function of Pressure

pressure (GPa)	peak position (cm^{-1})	FHWM (cm^{-1})
ambient	3484.45(1)	19.3(3)
0.184	3479(1)	10.0(3)
0.711	3457.26(4)	14.51(6)
1.555	3421.45(9)	15.53(9)
3.354	3351.68(7)	22.54(8)
5.106	3283.01(7)	22.68(9)
7.685[a]	N/A	N/A

[a]No well-defined stretching band observed in spectrum.

Table 6. D···A (Å) Distances for Hydrogen Bonds in $GaAsO_4{\cdot}2H_2O$ as a Function of Pressure (GPa), as Determined from High-Pressure Diffraction Measurements[a]

	ambient	2.405(6)	4.985(7)	6.927(8)
O5···O1	2.94(3)	2.99(3)	3.01(4)	3.03(3)
O5···O2^{iv}	2.65(2)	2.59(3)	2.58(4)	2.58(2)
O6···O4^{ii}	2.58(3)	2.57(3)	2.64(4)	2.53(3)

[a]Symmetry codes: (i) $x + 0.5, y, 1.5 - z$; (ii) $0.5 - x, y + 0.5$; (iv) $-x, 0.5 + y, 1.5 - z$. Note: D···H−A angles are not reported as the hydrogen atom positions could not be determined reliably; therefore, this information is meaningless.

which ultimately result in small distortions to the internal void spaces of the polyhedral helices that lie parallel to [010]. On the basis of the presented diffraction data, we have proposed a revised model for the hydrogen-bond network inherent in the solid-state structure of $GaAsO_4{\cdot}2H_2O$ and, most likely, in its isostructural analogues. This subsequently led to the reassignment of the ν(OH) peaks in previously published Raman spectra of this compound.

■ ASSOCIATED CONTENT

Supporting Information

Crystallographic information in CIF file. The Supporting Information is available free of charge on the ACS Publications website at DOI: 10.1021/acs.inorgchem.5b01144.

■ AUTHOR INFORMATION

Corresponding Author

*E-mail: nross@vt.edu.

Notes

The authors declare no competing financial interest.

■ ACKNOWLEDGMENTS

The authors acknowledge support from the National Science Foundation (Grant Nos. DMR-1206338 and EAR-1118691). E.C.S. thanks Dr. J. Zhao for technical assistance with the Raman measurements and Dr. R. Bodnar for access to the instrumentation.

■ REFERENCES

(1) Nordstrom, D. K. *Science* **2002**, *296*, 2143−2145.
(2) Smedley, P. L.; Kinniburgh, D. G. *Appl. Geochem.* **2002**, *17*, 517−568.
(3) Wang, S.; Mulligan, C. N. *Sci. Total Environ.* **2006**, *366*, 701−721.
(4) Le Berre, J.-F.; Gauvin, R.; Demopoulos, G. P. *Ind. Eng. Chem. Res.* **2007**, *46*, 7875−7882.
(5) Gomez, M. A.; Le Berre, J.-F.; Assaaoudi, H.; Demopoulos, G. P. *J. Raman Spectrosc.* **2011**, *42*, 62−71.
(6) Gomez, M. A.; Assaaoudi, H.; Becze, L.; Cutler, J. N.; Demopoulos, G. P. *J. Raman Spectrosc.* **2010**, *41*, 212−221.
(7) Yuan, Q.; Ren, S. L.; Zukowski, J.; Pomeroy, M.; Soghomonian, V. *Appl. Phys. Lett.* **2014**, *105*, 013904.
(8) Miletich, R.; Allan, D. R.; Kuh, W. F. *High-Temperature and High-Pressure Crystal Chemistry;* Hazen, R. M., Downs, R. T., Eds.; Mineralogical Society of America: Washington, DC, 2000; Vol. *41*, pp 445−519.
(9) Angel, R. J.; Allan, D. R.; Miletich, R.; Finger, L. W. *J. Appl. Crystallogr.* **1997**, *30*, 461−466.
(10) Angel, R. J.; Bujak, M.; Zhao, J.; Gatta, G. D.; Jacobsen, S. D. *J. Appl. Crystallogr.* **2007**, *40*, 26−32.
(11) Angel, R. J.; Finger, L. W. *J. Appl. Crystallogr.* **2011**, *44*, 247−251.
(12) Angel, R.; Gonzalez-Platas, J. *J. Appl. Crystallogr.* **2013**, *46*, 252−254.
(13) Mao, H. K.; Bell, P. M.; Shaner, J. W.; Steinberg, D. J. *J. Appl. Phys.* **1978**, *49*, 3276−3283.
(14) Angel, R. J.; Gonzalez-Platas, J.; Alvaro, M. *Z. Kristallogr. - Cryst. Mater.* **2014**, *229*, 405−419.
(15) Fan, D.; Ma, M.; Wei, S.; Li, B.; Chen, Z.; Xie, H. *High Temp. High Press.* **2013**, *42*, 203−209.

DOI: 10.1021/acs.inorgchem.5b01144
Inorg. Chem. 2015, 54, 7548−7554

(16) Christie, D. M.; Chelikowsky, J. R. *J. Phys. Chem. Solids* **1998**, *59*, 617−624.
(17) Gibbs, G. V.; Ribbe, P. H.; Robinson, K. *Science* **1971**, *172*, 567−570.
(18) Yang, J.; Zhao, Y.; Frost, R. L. *Spectrochim. Acta, Part A* **2009**, *74*, 398−403.
(19) Frost, R. L.; Kloprogge, J. T. *Spectrochim. Acta, Part A* **2003**, *59*, 2797−2804.
(20) Libowitzky, E. *Monatsh. Chem.* **1999**, *130*, 1047−1059.
(21) Winkler, B. Hydrogen Bonding in Minerals at High Pressure. In *High-Pressure Crystallography: From Fundamental Phenomena to Technological Applications;* Boldyreva, E., Dera, P., Eds.; Springer: New York, 2010; pp 493−501.
(22) Angel, R. J. *Contrib. Mineral. Petrol.* **2004**, *146*, 506−512.
(23) Downs, R. T.; Yang, H.; Hazen, R. M.; Finger, L. W.; Prewitt, C. T. *Am. Mineral.* **1999**, *84*, 333−340.
(24) Benusa, M. D.; Angel, R. J.; Ross, N. L. *Am. Mineral.* **2005**, *90*, 1115−1120.

DOI: 10.1021/acs.inorgchem.5b01144
Inorg. Chem. 2015, 54, 7548−7554